Influence of laser shock peening on the residual strains and stresses in additively manufactured TC4

Mariia L. Bartolomei, Aleksei N. Vshivkov, Igor S. Kudryashev, Denis V. Lozhkin
Institute of Continuous Media Mechanics of the Ural Branch of Russian Academy of Science (ICMM UB RAS), Russia
bartolomei.m@icmm.ru, http://orcid.org/0009-0003-3193-7605
vshivkov.a@icmm.ru, http://orcid.org/ 0000-0002-7667-455X
i.s.kudryashev@gmail.com, http://orcid.org/ 0009-0009-2284-7388
lozhkin.d@icmm.ru, http://orcid.org/ 0000-0003-3302-8408

Andrey V. Chumaevskii
Institute of Strength Physics and Materials Science of the Siberian Branch of Russian Academy of Science, Russia
tch7av@gmail.com, http://orcid.org//0000-0002-1983-4385

Alexander M. Korsunsky
HSM Lab, Skolkovo Institute of Science and Technology, Russia
CASM&T, Advanced School of Engineering, Moscow Aviation Institute, Russia
a.korsunsky@skoltech.ru, http://orcid.org/0000-0002-3558-5198

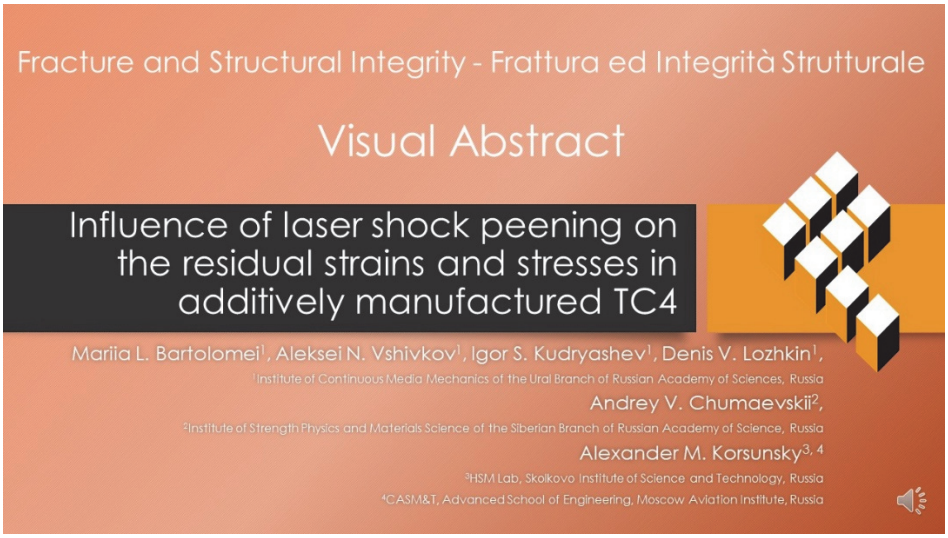

Citation: Bartolomei, M. L., Vshivkov, A. N., Kudryashev, I. S., Lozhkin, D. V., Chumaevskii, A. V., Korsunsky, A. M., Influence of laser shock peening on the residual strains and stresses in additively manufactured TC4, Fracture and Structural Integrity, 75 (2026) 35-45.

Received: 25.09.2025
Accepted: 08.10.2025
Published: 16.10.2025
Issue: 01.2026

KEYWORDS. Additively manufactured TC4, Residual strains, Residual stresses, Laser shock peening.

INTRODUCTION

Additive manufacturing (AM), commonly known as 3D printing, has revolutionized the production of metal parts by enabling the layer-by-layer fabrication of complex geometries directly from digital models. Techniques such as selective laser melting (SLM) and electron beam melting (EBM) offer unparalleled design freedom, significant material savings, and reduced waste compared to traditional subtractive methods [1]. This has led to rapid and widespread adoption across aerospace, medical, and automotive industries.

However, the very nature of AM, with its rapid melting and solidification cycles, introduces significant challenges. The extreme thermal gradients may cause detrimental residual stresses to develop in the surface layers of the fabricated parts. These stresses can compromise the component's mechanical integrity, leading to reduced strength, durability, and potential distortion or cracking. Furthermore, additively manufactured materials often exhibit microstructures with anisotropic properties, i.e. differing between the laser scanning direction, the material growth direction and the third transverse direction [2, 3]. Furthermore, AM may lead to the formation of defects such as pores and microcracks [4].

To enhance the surface characteristics of AM prints and to eliminate volumetric defects, various post-processing techniques are employed, including heat (and pressure) treatment, shot peening, grinding, and laser shock peening (LSP) [5-7]. This work focuses on LSP as an advanced surface treatment technology using high-power laser pulses to generate shock waves at the surface of a material. These waves induce plastic deformation, thereby work-hardening the surface layer. This technology is particularly promising for introducing beneficial compressive residual stresses in the near-surface layers of additively manufactured components [8], which are crucial for improving fatigue life [9-11]. LSP finds application in the aerospace [12], automotive, and energy industries when wear resistance and part fatigue strength are critical. Its advantages include minimal thermal impact on the treated part and the ability to adjust precisely the processing parameters (such as pulse energy and number of passes) for different materials [13].

LSP treatment is based on the effect of hot plasma formation at a surface subjected to high-energy impact. The sample surface is first coated with a protective ablative layer, such as black paint, metallic foil, or PVC tape. A laminar flow of a transparent (weakly absorbing) fluid (typically water) is then applied over the treated surface. The laser beam passes through the water confining layer and strikes the absorbing layer. The absorbed energy causes a portion of the protective layer to vaporize, and then to form a high-temperature plasma. This plasma undergoes adiabatic expansion, generating significant pressure at the material surface and initiating a shock wave within the material volume.

The pressure pulse duration depends on both the radiation pulse duration and the specific process conditions. The use of a water confining layer enables the generation of elastic-plastic waves with an amplitude ranging from units to tens of GPa. Simple estimates based on a one-dimensional plasma expansion model allows estimating the plasma pressure decay, namely, that it halves after twice the interaction time between the pulse and the material and decreases tenfold after approximately 15 characteristic times. If the pressure induced by the plasma expansion exceeds the material's dynamic yield strength, plastic deformation occurs, resulting in residual stresses. The resulting compressive residual stresses at the surface are balanced by tensile stresses in the material core.

Laser shock peening is a complex process with a large number of variable parameters, such as laser energy, beam shape and size, degree of overlap between adjacent pulses, and the number of repeated impacts. All these parameters significantly influence the quality of the final result.

The aim of the present work is to determine the relationship between the magnitude and depth of relief strains in samples made from TC4 titanium alloy produced by wire-feed electron-beam additive manufacturing and various parameters of laser shock peening (power density, beam shape, overlap). The obtained results serve to validate a numerical model of both the manufacturing and laser shock peening processes for this material. The verified model will enable the prediction of residual stress fields in additively manufactured components with complex geometries, where traditional hole-drilling techniques are not applicable.

LASER SHOCK PEENING AND RESIDUAL STRAINS MEASUREMENT

The laser shock peening system, developed at the Institute of Continuous Media Mechanics of the Ural Branch of Russian Academy of Science (ICMM UB RAS), incorporates a Beamtech SGR-Extra-10 solid-state Nd:YAG laser with a wavelength of 1064 nm, a maximum pulse repetition rate of 5 Hz, a maximum pulse energy of 9 J, and a pulse duration of 10 ns. The beam shape at the laser output is a circle with a diameter of 25 mm. The beam can be focused using additional lenses to achieve the following spot geometries: a circle with a diameter of 2 mm, a 1x1 mm

square, or a 3x3 mm square. As a result, the maximum achievable power density (impact) generated by this system is 90 GW/cm².

Laser operation is controlled automatically by a robotic manipulator. The six-axis STEP SR50 robotic manipulator, with a payload capacity of 50 kg and a part positioning accuracy of 0.25 mm (Fig. 1), enables automated processing of parts with complex geometries. During the process, the manipulator automatically positions the workpiece in front of the laser beam so that the beam strikes the surface at a normal angle; it then sends a TTL signal to the laser system to trigger a pulse.

The manipulator moves the part at a specified speed within a range of 0.1 mm/s to 500 mm/s and ensures high accuracy in directing the laser pulses to predetermined points on the part's surface. The laser beam path trajectories are generated by specialized software based on the 3D model of the part.

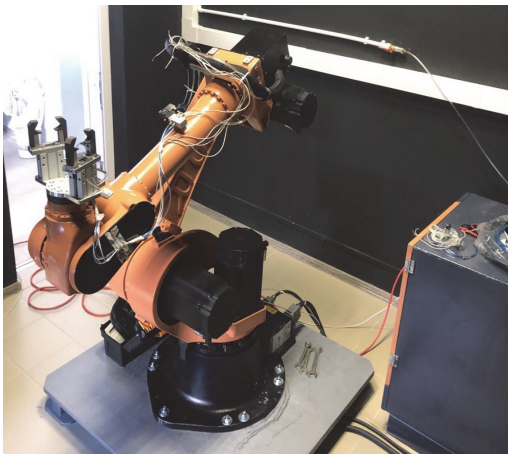

Figure 1: STEP SR50 robotic manipulator.

The resulting residual stresses are evaluated using the MTS3000 – Restan automated residual stress measurement system (Fig. 2). This system is used to perform simple and precise measurements by the hole-drilling strain gauge method using a high-speed air turbine (400,000 rpm) in accordance with the ASTM E837 [14-15] standard. A strain gauge rosette (a characteristic size of 10 mm) with three measuring grids is installed on the surface of the sample, and a hole 1-2 mm in diameter is drilled at a specific location on it. Drilling is performed stepwise; at the end of each step, the strain gauge records the values of hole deformations arising from the relief of compressive residual stresses. The measurement error does not exceed 1 μm/m.

The method for measuring residual strains includes the following steps:

1. Preparation of the specimen surface by polishing prior to strain gauge installation.
2. Degreasing of the surface.
3. Applying alignment markings for the strain gauge on the surface.
4. Bonding the strain gauge to the specimen surface using cyanoacrylate adhesive.
5. Connecting the gauge to a signal amplifier.
6. Launching the RSM software.
7. Centering the automated system using a digital microscope.
8. Automated search for the specimen surface.
9. Checking the signals coming from the strain gauge.
10. Initiating the automated step-by-step hole drilling.

The obtained data is used to solve an inverse problem, the result of which is a depth profile of the residual stresses. It should be noted that residual stresses with a level close to the material proportional deformation limit are estimated rather roughly and require adjustment. To obtain reliable data, the area with residual stresses must be larger than the measuring strain gauge rosette. The method makes it possible to obtain an averaged value of residual stresses based on the strain sensor measurement.

The Non-Uniform Stress Field method was used to calculate the residual stresses [16]. This is a standardized approach for determining residual stresses in a material using the hole drilling method, which accounts for the non-uniform stress distribution with depth. This method is part of the internationally recognized ASTM E837 standard, which is officially endorsed and applied in both industrial and research practice. This standard implies a variety of algorithms, with strain being

the primary experimental result. Since this data can be utilized by other researchers for accurate calculations, the experimental part of this work focuses on measuring strains.

Unlike the simplified uniform stress field variant, which assumes a constant stress throughout the hole depth, this method allows for the evaluation of how residual stresses vary with depth layer by layer. This is particularly important in the case of surface treatments, welding, grinding, hardening, and other processes that induce a variable distribution of internal stresses. The residual stresses present in the material prior to drilling are evaluated based on the measured relaxed strains (ε_1, ε_2, and ε_3) at each depth increment (j) of the hole and using linear elastic material model. In fact, residually stressed states represent the solution of continuum elastic problem in the presence of inelastic strain perturbation, also known as *eigenstrain* [17]. The problem of finding the inherent eigenstrain distribution in the materials and then reconstructing the complete stress-strain distribution is known as the inverse problem of *eigenstrain*. The calculated stresses along the strain gauge axes are denoted as σ_1 and σ_3, and the shear stress oriented at a 45° angle is denoted as τ_{13}.

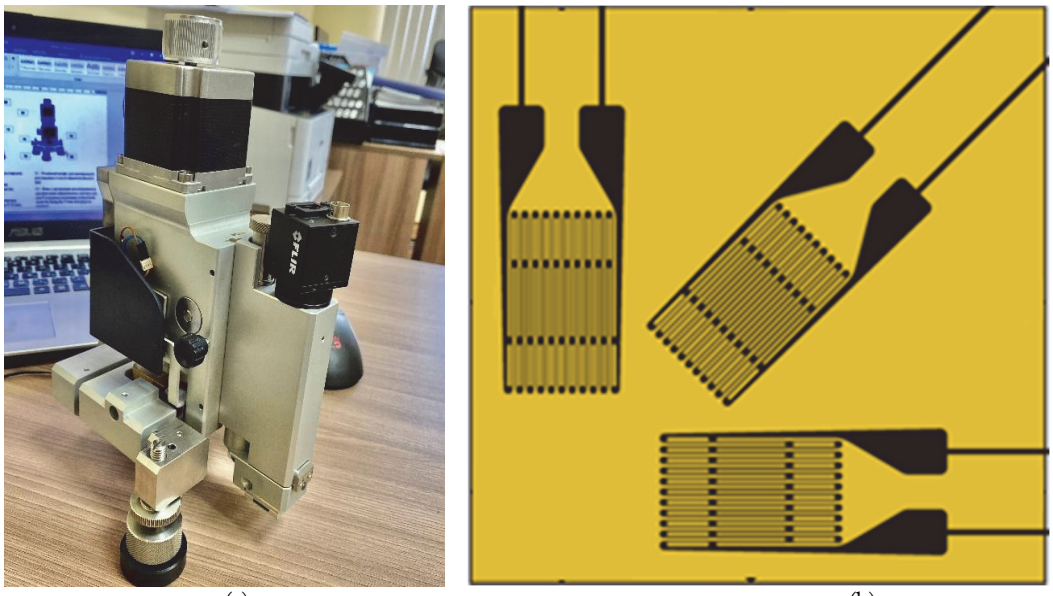

(a) (b)

Figure 2: MTS3000-Restan Residual Stress Measurement System by the hole drilling method (a), schematic illustration of the 45° triple gauge rosette with gauges oriented at 0°, 45° and 90° (b).

RESULTS AND DISCUSSION

The subject of the study were plate specimens with the maximum thickness of 7 mm with a gently thinned down part of thickness 5 mm. The specimens were used to determine the influence of the processing parameters on the distribution of relief strains. All specimens were cut from TC4 titanium alloy produced by using wire-feed electron beam additive manufacturing [18]. Fig. 3 shows the specimen geometry.

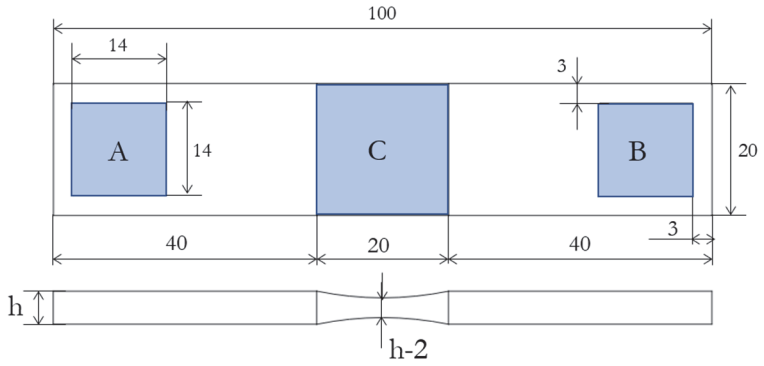

Figure 3: Geometry of the plate specimens with the processed areas indicated: (A, B) for measuring residual strains by the hole drilling method on the thicker part of the sample; (C) thinned down area for the determination of fatigue properties.

The specimens investigated were cut from the workpiece in two directions: along the printing (scanning) direction X in the workpiece (Fig.4) and along the build direction Z of the workpiece. The workpiece was a rectangular wall fabricated by scanning in the horizontal X direction and growth in the vertical direction Z. The locations from which the specimens were extracted are shown schematically in Fig. 4.

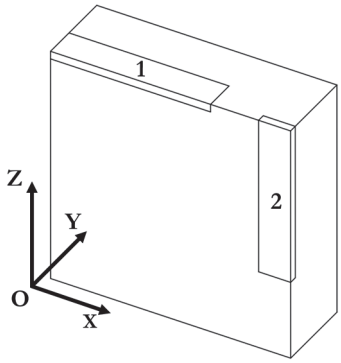

Figure 4: Schematic illustration of the sample location within the workpiece: 1 – Horizontal (along the printing direction of the workpiece); 2 – Vertical (along the build direction of the workpiece). X is the printing (scanning) direction, and Z is the build direction.

Fig. 5 shows a photo of the sample on the robotic manipulator during the processing of areas A and B (as shown in Fig. 3) for the measurement of relief strains. The sample was mounted on the fixture plate using double-sided adhesive tape. Since the treatment area is significantly smaller than the sample dimensions, its deformation during treatment does not affect the quality of the mounting achieved by this method. To ensure precise and repeatable sample positioning, locating pins were placed on the fixture plate.

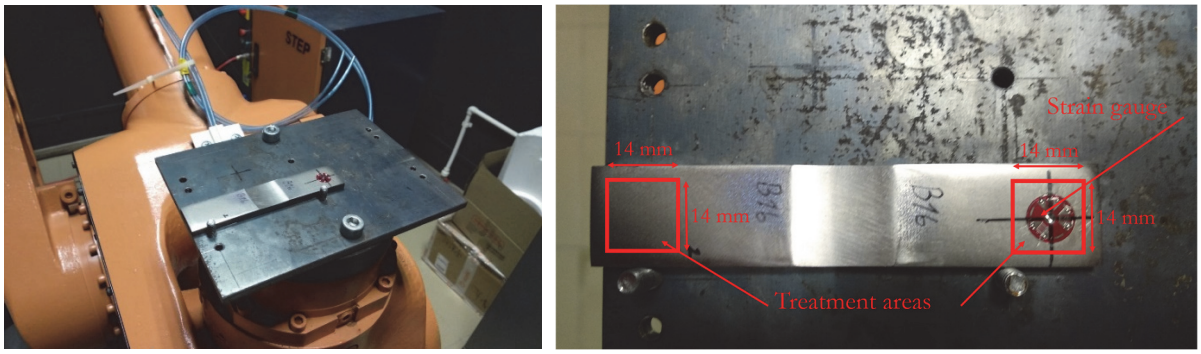

(b) (b)

Figure 5: Sample photo on a robotic manipulator (a), designation of the treatment area for measuring discharge strains (b).

To evaluate the influence of the process parameters on the residual stress profile, five processing regimes were implemented to cover a wide range of parameters. During processing, 80 μm thick adhesive-backed aluminum foil was used as the cover layer. The laser pulse repetition rate was set to 5 Hz. A series of flat samples was processed, and the depth profile of residual strains was measured. The investigated laser shock peening regimes and obtained results for the samples are presented in Tab. 1. Spots of two sizes were considered: a circle with a diameter of 2 mm (D2) and a square measuring 1 by 1 mm (1x1). The depth distribution of the residual strains for the as-build specimens sectioned from the workpiece (as illustrated in Fig. 4) is presented in Fig. 6 for the X and Z samples (denoted by the sample long axis orientation with respect to the system of coordinates of Fig. 4). The plots adhere to the following convention: ε1 denotes the strain component along the sample length, and ε2 denotes the transverse strain component.

Fig. 6 shows that the relief strains as a function of drilling depth in the build direction specimens are almost an order of magnitude greater than those in the printing direction specimens. Furthermore, for the build direction specimens, the highest strain intensity is observed at a depth of 0.2 – 0.3 mm, whereas in the printing direction specimens, it is more uniform up to a depth of 0.6 mm.

A characteristic view of the relief strains measured by strain gauges during the incremental drilling process is shown in Fig. 7.

№	Processing direction	Overlap, %	Energy, J	Power density, GW/cm²	Spot shape	Surface residual strain, μS	Max residual strain, μS	Residual strain depth, mm
1	Printing	-	-	-	-	-3.60	5.30	0.55
2	Printing	30	2	6.37	D2	-1.55	28.40	0.30
3	Printing	30	4	12.74	D2	-2.32	34.93	0.30
4	Printing	30	6	19.11	D2	11.75	31.50	0.35
5	Printing	0	1	10	1x1	12.10	39.30	0.20
6	Printing	0	2	20	1x1	-13.04	56.15	0.20
7	Build	-	-	-	-	-20.50	16.30	0.30
8	Build	30	2	6.37	D2	7.95	33.90	0.20
9	Build	30	4	12.74	D2	16.81	45.77	0.25
10	Build	30	6	19.11	D2	15.10	42.20	0.30
11	Build	0	1	10	1x1	16.25	38.20	0,25
12	Build	0	2	20	1x1	7.10	35.30	0.30

Table 1: The investigated LSP regimes.

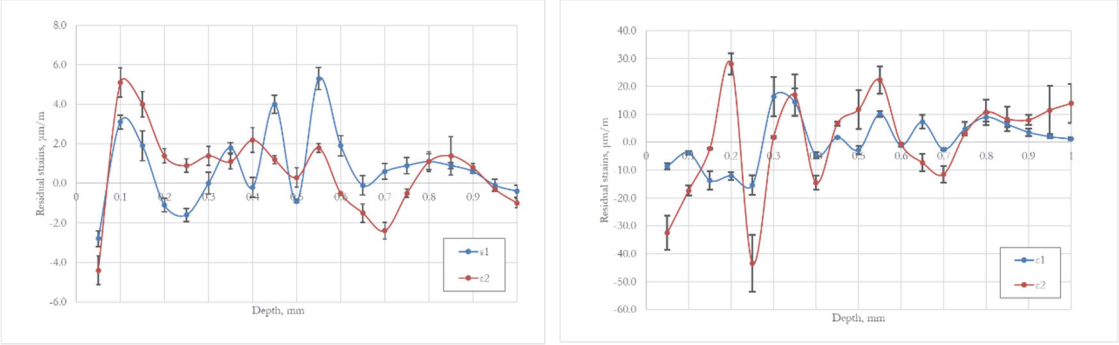

(a) (b)

Figure 6: Residual strains distribution for as-build specimens along the printing direction (a), along the build direction (b).

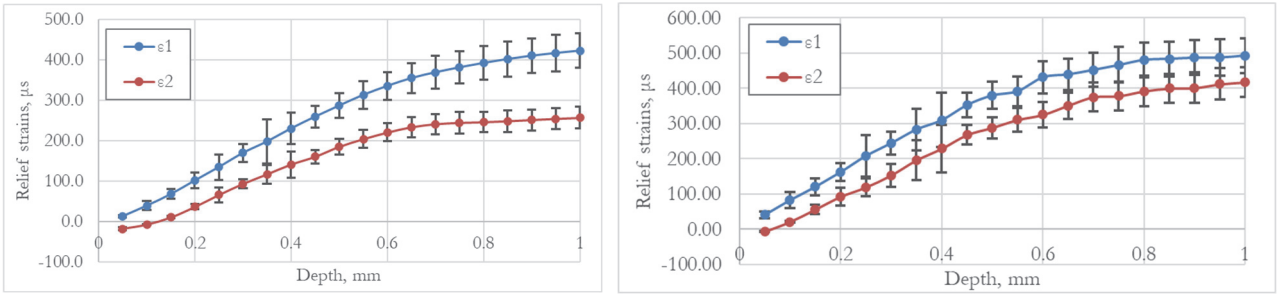

(a) (b)

Figure 7: Characteristic relief strains measured by the hole drilling method in specimens treated with a spot of D2 mm and a power density of 12.74 GW/cm² for specimens along the printing direction (a), along the build direction (b).

The plots in Fig. 7 reflect the overall material response to the sequential release of residual stresses during hole drilling. Some divergence in the strain components is observed, likely associated with the directional variation of the printed material microstructure and properties. Fig. 8 shows a characteristic dependence of residual strains on depth.

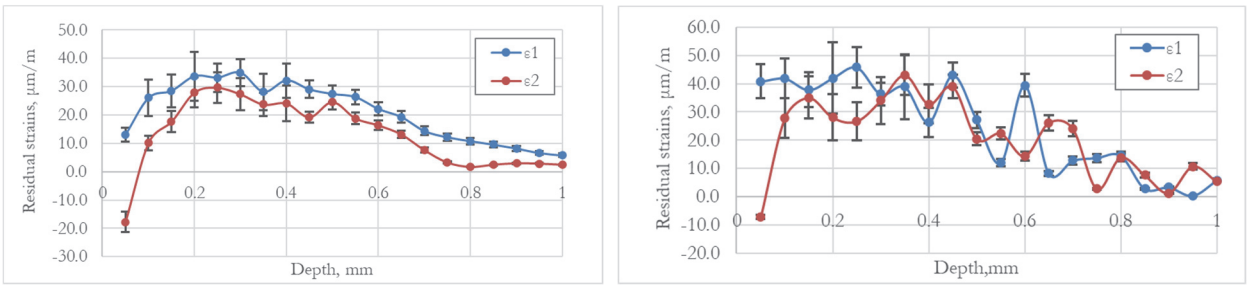

(a) (b)

Figure 8: Characteristic residual strains patterns in specimens treated with a spot of D2 mm and a power density of 12.74 GW/cm² for specimens along the printing direction (a), along the build direction (b).

A positive value of the relief strains indicates the presence of compressive residual stresses [19]. In general, for all treatment regimes, compressive stresses are observed at a depth of up to 1 mm, with the maximum amplitude at a depth of approximately 0.2 – 0.4 mm.

Figs. 9 and 10 show the dependences of the total strain and the maximum relief strain on the laser pulse power density for specimens along the printing direction and along the build direction processed with a square beam (1x1) and a round beam (D2).

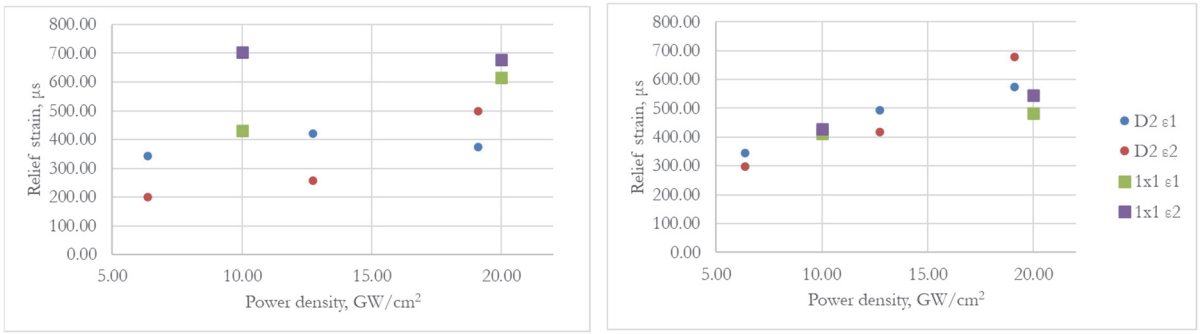

(a) (b)

Figure 9: The relationship between the relief strains and the laser pulse power density for specimens along the printing direction (a), along the build direction (b).

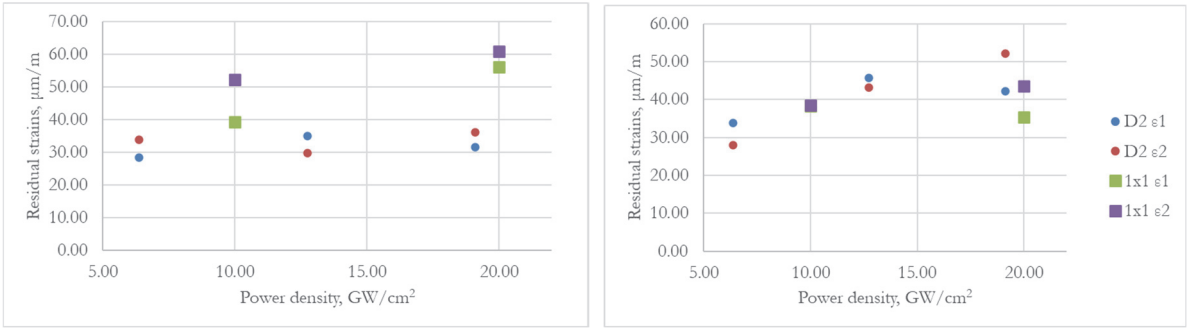

(a) (b)

Figure 10: The relationship between the maximum residual strains and the laser pulse power density for specimens along the printing direction (a), along the build direction (b).

For specimens along the build direction, a more pronounced dependence of strain on the laser pulse power density is observed. For specimens along the printing direction, exposure with a square beam yields a better effect. This is likely due to the initial properties of the specimens and is related to the direction of the workpiece growing. Relief strains increase nonlinearly with the growth of the laser pulse power density. At power densities above 12-15 GW/cm², this growth is no longer as evident. The graphs of residual stress dependence on depth show similar patterns as those for residual strains, see Fig. 11.

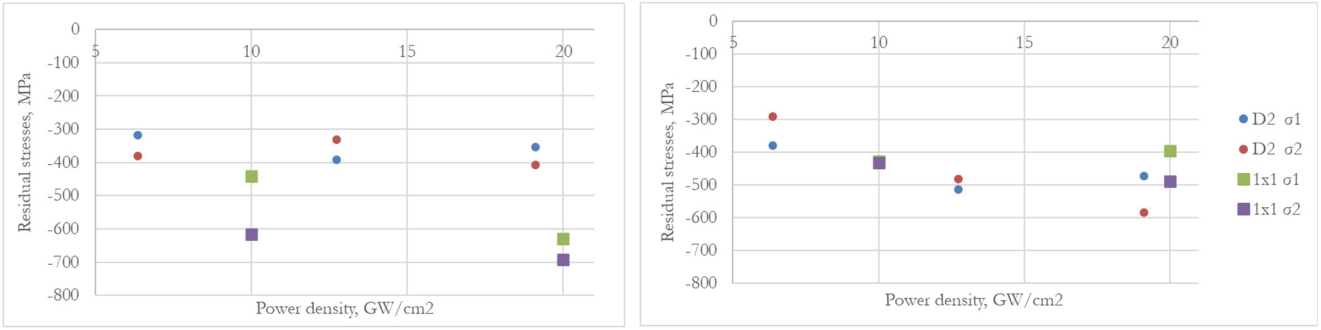

(a) (b)

Figure 11: The relationship between the maximum residual stresses and the laser pulse power density for specimens along the printing direction (a), along the build direction (b).

NUMERICAL MODELING OF RESIDUAL STRESS FORMATION

Finding the optimal combination of parameters for LSP of a specific material requires a detailed investigation. This is because LSP is a complex surface treatment technology involving a large number of variable parameters. Coupled with mathematical modeling, the selection of the required processing parameters will ensure high quality of the resulting product, including the depth and magnitude of compressive residual stresses in components of arbitrary geometry. Thus, experimental data on residual stresses and strains in additively manufactured specimens were used to validate the numerical model.

To ensure that the residual stress in the numerical model sample (Fig. 12) corresponded to that in a sample extracted from an additively manufactured workpiece, a material with the properties listed in Tab. 2 was grown in the Ansys Mechanical package. To simulate the dynamic material deformation under this loading, the stress-strain state was calculated in Ansys LS-Dyna. The Johnson-Cook model was adopted as the constitutive relation [20-22].

Beam current for perimeter printing, mA	Beam current for infill, mA	Scan speed, mm/min	Wire feed rate, mm/min	Wire filament diameter, mm	Nominal layer height, mm	Hatch spacing, mm
57	65	400	1528	1.6	1.5	3

Table 2: Main printing parameters for samples made of TC4 titanium alloy.

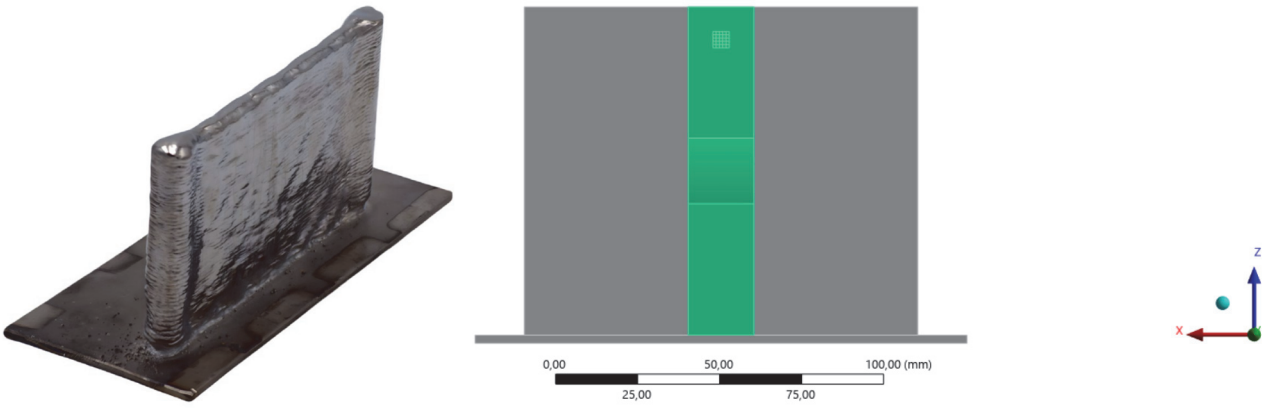

Figure 12: The specimen location on the additively manufactured workpiece.

The stress state from the workpiece was imported from the Static Structural module into LS-Dyna. The sample was treated in a 5x5 mm area using a square laser spot with a side of 1x1 mm and an energy density of 20 GW/cm². The sample, indicating the processing direction and finite element discretization, is shown in Fig. 13. The element size in the peening

zone was 0.15 mm and gradually increased towards the specimen boundaries up to 2 mm. The laser pulse had a rise time of 40 ns and a fall time of 60 ns. The lower boundary of the specimen was fixed.

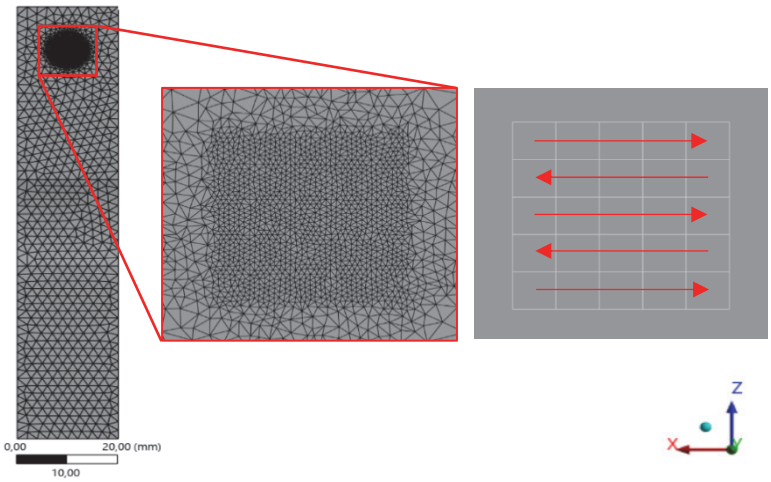

Figure 13: The finite element discretization and processing direction.

A comparison of the residual strains profiles in a specimen cut from a workpiece after building and before LSP treatment is shown in Fig. 14a. The component ε1 in the direction along the sample was compared. The resulting distribution of residual stresses after the LSP for component σ1 is shown in Fig. 14b, the distribution of residual stresses was measured in the middle of the impact spot.

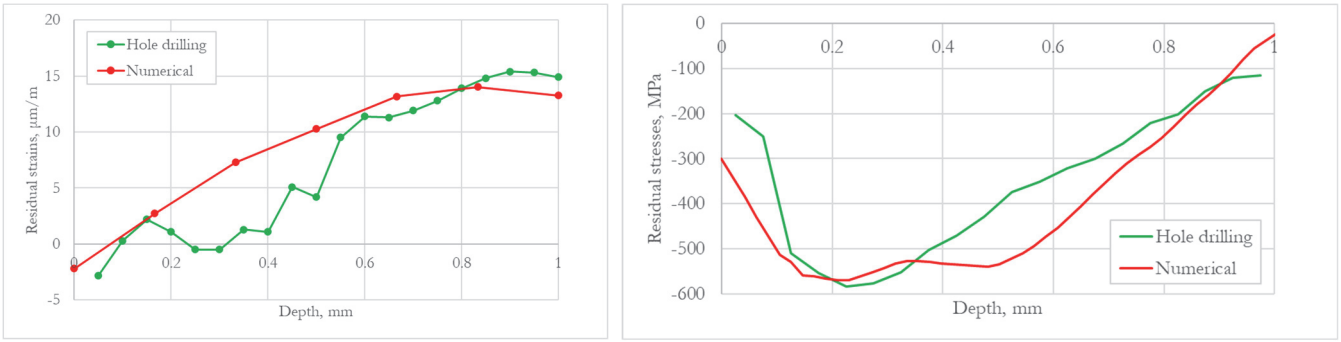

(a) (b)

Figure 14: Comparison of depth distribution of residual strains for component ε1 (a), of residual stresses for component σ_1 (b) for specimens along the printing direction.

Based on the comparison of the residual strain profiles in the sample (machined from the base material and the as-built additively manufactured material prior to treatment) and the residual stresses induced after treatment, it can be concluded that the numerical model accurately describes the data obtained from hole-drilling method, both qualitatively and quantitatively, with an error margin not exceeding 10%. Consequently, numerical simulation enables the evaluation of stress and strain values in parts with complex geometries where the hole-drilling method is inapplicable (e.g., for parts with a thickness of less than 1 mm or with curved surfaces). This, in turn, facilitates a faster and more precise selection of the optimal processing parameters for the material and component under investigation.

Conclusions

The purpose of this work was the analysis the effect of LSP parameters on the residual stress and strain profiles in samples of TC4 titanium alloy. The samples were produced by cutting and machining workpieces of additively manufactured material. The hole-drilling method revealed the presence of tensile residual stresses in the additively

manufactured samples. Experimental data on the residual deformations were obtained. These data can be used by other researchers to develop methods for calculating residual stresses. The authors in their earlier work defined a data processing algorithm for residual stress calculation. After LSP, the formation of compressive residual stresses in the structure was experimentally demonstrated. The presence of compressive stresses induced by LSP will also lead to porosity closure and an increase in the fatigue life of the component, thus demonstrating the effectiveness of this post-processing technique for additive materials.

The laser power density was varied within the range of 6 to 20 GW/cm². It is shown that the process efficiency decreases at a laser power density exceeding 10–15 GW/cm². The maximum residual strains reach 50 μm/m at a depth of 0.2–0.4 mm. The total depth of the deformed layer is at least 1 mm.

A numerical model was developed to describe the manufacturing and LSP treatment of additively fabricated components. The hardening model used in the calculations does not consider the plasma formation process, which generates high pressure. Instead, it describes hardening via residual stresses induced in the material by elastic-plastic waves resulting from its expansion. The model enables both qualitative and quantitative assessment of residual stresses and deformations in a structure of arbitrary geometry for a given processing regime. Therefore, this numerical model will enable a more detailed analysis of residual stress and strains distribution in additively fabricated structures.

ACKNOWLEDGMENTS

This study was carried out under the Agreement for the provision of grant funding from the federal budget for large scientific projects in priority areas of scientific and technological development of the Russian Ministry of Science and Higher Education no. 075-15-2024-552

REFERENCES

[1] Andreacola, F. R., Capasso, I., Pilotti, L., Brando, G. (2021). Influence of 3d-printing parameters on the mechanical properties of 17-4PH stainless steel produced through Selective Laser Melting. Fracture and Structural Integrity, 15(58), pp. 282–295. DOI: https://doi.org/10.3221/IGF-ESIS.58.21.

[2] Schillaci, C., Pilone, D., Berto, F., Bellini, C., Di Cocco, V., Di Giamberardino, P., & Iacoviello, D. (2025). Correlation Between Process Parameters and Mechanical Properties of Ti6Al4V Alloys Processed by Electron Beam Melting. Fracture and Structural Integrity, 19(74), pp. 310–320. DOI: https://doi.org/10.3221/IGF-ESIS74.19.

[3] Klimenov V.A., Kolubaev E.A., Han Z, Chumaevskii A.V., Dvilis E.S., Strelkova I.L., Drobyaz E.A., Yaremenko O.B., Kuranov A.E. (2023) Elastic modulus and hardness of Ti alloy obtained by wire-feed electron-beam additive manufacturing. Obrabotka metallov (tekhnologiya, oborudovanie, instrumenty) = Metal Working and Material Science, 25(4), pp. 180–201. DOI: https://doi.org/10.17212/1994-6309-2023-25.4-180-201. (In Russian)

[4] Tan, K., Yeo, S. (2020). Surface finishing on IN625 additively manufactured surfaces by combined ultrasonic cavitation and abrasion, Additive Manufacturing, 31, 100938. DOI: https://doi.org/10.1016/j.addma.2019.100938.

[5] Maleki, E., Shamsaei, N. (2024). A comprehensive study on the effects of surface post-processing on fatigue performance of additively manufactured AlSi10Mg: An augmented machine learning perspective on experimental observations, Additive Manufacturing, 86. 104179. DOI: https://doi.org/10.1016/j.addma.2024.104179.

[6] Ye, C., Zhang, C., Zhao, J. et al. (2021). Effects of Post-processing on the Surface Finish, Porosity, Residual Stresses, and Fatigue Performance of Additive Manufactured Metals: A Review. J. of Materi Eng and Perform 30, pp. 6407–6425. DOI: https://doi.org/10.1007/s11665-021-06021-7.

[7] Steinhauser, M., Sert, E., Hitzler, L., Öchsner, A. and Merkel, M. (2020). Fatigue Behavior of the Additively Manufactured Tool Steel H13 after Surface Treatment using Different Post-Processing Methods. Practical Metallography, 57(3), pp. 140-167. DOI: https://doi.org/10.3139/147.110599.

[8] Lan, L., Xin, R., Jin, X., Gao, S, He, B., Rong, Y., Min, N. (2020). Effects of Laser Shock Peening on Microstructure and Properties of Ti-6Al-4V Titanium Alloy Fabricated via Selective Laser Melting, Materials (Basel), 13(15), 3261. DOI: https://doi.org/10.3390/ma13153261.

[9] Zha, S., Zhang, H., Yang, J., Zhang, Z., Qi, X., Zu, Q. (2025). Fatigue Threshold and Microstructure Characteristic of TC4 Titanium Alloy Processed by Laser Shock, Metals, 15 (453). DOI: https://doi.org/10.3390/met15040453.

[10] Pan, X., Li, X., Zhou, L., Feng, X., Luo, S., He, W. (2019). Effect of Residual Stress on S–N Curves and Fracture Morphology of Ti6Al4V Titanium Alloy after Laser Shock Peening without Protective Coating, Materials, 12 (3799). DOI: https://doi.org/10.3390/ma12223799.
[11] Yang, S., Hu, W., Zhan, Z., Li, J., Bai, C., Yang, Q., Meng, Q. (2022). Fatigue tests and a damage mechanics-based fatigue model on a cast Al-Si-Mg aluminum alloy with scratches, International Journal of Fatigue, 165, 107198. DOI: https://doi.org/10.1016/j.ijfatigue.2022.107198.
[12] Fameso, F., Desai, D., Kok, S., Armfield, D., Newby, M. (2022). Residual Stress Enhancement by Laser Shock Treatment in Chromium-Alloyed Steam Turbine Blades, Materials, 15 (5682). DOI: https://doi.org/10.3390/ma15165682.
[13] Sundar, R. (2022). Laser Shock Peening: A Walkthrough. In: Radhakrishnan, J., Pathak, S. (eds) Advanced Engineering of Materials Through Lasers. Advances in Material Research and Technology. Springer, Cham. DOI: https://doi.org/10.1007/978-3-031-03830-3_4.
[14] ASTM E837-01. Standard Test Method for Determining Residual Stresses by the Hole-Drilling StrainGage Method, Annual ASTM book of standards available at: http://www.astm.org.
[15] Rendler, N.J., Vigness, I. (1966). Hole-drilling strain-gage method of measuring residual stresses, Experimental Mechanics. 6, pp. 577–586. DOI: https://doi.org/10.1007/BF02326825.
[16] Viotti, M., Albertazzi, A. (2103). Approximated Repair Methods for Outlier Strain Data from Hole-Drilling Residual Measurements, Experimental Mechanics, 53, pp. 393–403. DOI: https://doi.org/10.1007/s11340-012-9642-0.
[17] Korsunsky, A.M. (2017) A Teaching Essay on Residual Stresses and Eigenstrains. Butterworth-Heinemann, ISBN 978-0-12-810990-8.
[18] Chumaevskii, A., Tarasov, S., Gurianov, D., Moskvichev, E., Rubtsov, V., Savchenko, N., Panfilov, A., Korsunsky, A.M., Kolubaev, E. (2024). Analysis of the Structure and Properties of As-Built and Heat-Treated Wire-Feed Electron Beam Additively Manufactured (WEBAM) Ti–4Al–3V Spherical Pressure Vessel, Metals, 14, 1379. DOI: https://doi.org/10.3390/met14121379.
[19] Totten, G. E., Howes, M. A. H., & Inoue, T. (2002). *Handbook of residual stress and deformation of steel.* ASM International.
[20] Braisted, W., Brockman, R. (1999). Finite element simulation of laser shock peening, Int. J. Fatigue, 21, pp. 719-724. DOI: https://doi.org/10.1016/S0142-1123(99)00035-3.
[21] Keller, S., Chupakhin., S., Staron, P., Maawad, E., Kashaev, N. and Klusemann, B. (2018). Experimental and numerical investigation of residual stresses in laser shock peened AA2198, J. Mater. Process. Technol., 255, pp. 294-307. DOI: https://doi.org/10.1016/j.jmatprotec.2017.11.023.
[22] Bartolomei, M. L., Kudryashev, I. S., Sabirov, R. R., & Korsunsky, A. M. (2025). Numerical study of residual stress fields after double-sided symmetric laser shock peening of blade edge, Fracture and Structural Integrity, 19(72), pp. 26–33. DOI: https://doi.org/10.3221/IGF-ESIS.72.03.